

Connections between rate-induced tipping and nonautonomous stability theory

Alanna Hoyer-Leitzel, Alice Nadeau, Andrew Roberts and Andrew Steyer

February 13, 2017

Abstract

We discuss the phenomenon of rate-induced tipping, where changing a parameter past a critical rate causes the system to ‘tip’ or diverge from an attractor, within the framework of nonautonomous stability theory. We explore rate-induced tipping in several one-dimensional model nonautonomous systems using finite time Lyapunov exponents and Steklov averages. Our results show that these numerical stability spectra are effective diagnostics for determining rate-induced tipping points in systems with parameters that are asymptotically constant or are linear. We then apply these stability spectra to a conceptual climate model.

Keywords: Tipping, Rate Tipping, Nonautonomous Dynamical Systems, Bifurcations, Compost Bomb

1 Introduction

The applications of tipping points to the study of climate are widespread and important (see [1] and references therein). Knowing how and when a system tips has ramifications for climate systems. Previous studies of rate-tipping use analytical techniques (give example) to characterize rate-tipping for low dimensional systems with time-dependent parameters that are asymptotically constant [2]. In this paper we explore the relationship between rate-induced tipping and nonautonomous stability theory. Furthermore, we exploit this relationship to use a numerical indicator of stability to detect rate-induced tipping points in low-dimensional systems with parameters that are changing at a constant rate.

1.1 Rate-induced Tipping

Tipping points are characterized by a sudden shift in the behavior of the system due to a relatively small change in inputs [22, 31]. Generally these changes transform the solution of the system in a significant qualitative manner (e.g., switching to a different equilibrium solution) and often the result is difficult, or even impossible, to reverse, making the study of predicting and preventing this tipping phenomenon highly important. Ashwin et al (2012) [2] classified tipping phenomena into three categories based on the mechanism causing the tipping. Tipping may result from

- *bifurcations* in state space,
- *noise*, where noise within the system causes a change in state, and
- *rate*, where the rate at which a parameter is changing causes a change in state.

We give pictorial examples of the types of tipping in Figure 1.

In this paper we focus on rate-induced tipping. We look at examples of systems of the form $x \in \mathbb{R}^n$,

$$\dot{x} = f(x, \lambda(t)) \tag{1}$$

where $\lambda(t)$ is a function of t which is as smooth as the system, at least C^1 . In the case where $\lambda(t)$ is constant, $f(x, \lambda) = 0$ gives equilibrium points for the associated autonomous system. The time-dependent solutions to $f(x, \lambda(t)) = 0$, while not solutions to the nonautonomous dynamical system, still attract or repel solutions

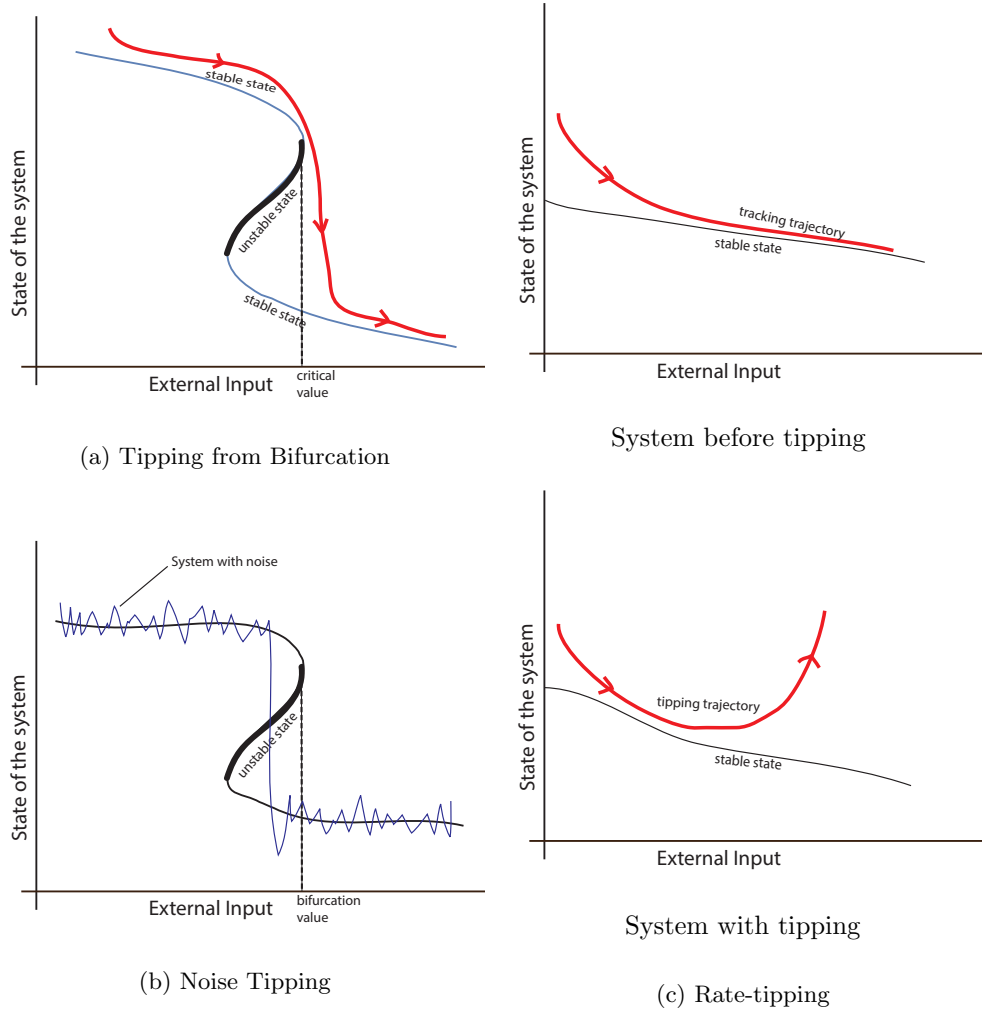


Figure 1: Examples of the types of tipping given by Ashwin et al. [2]. In (a) we see a trajectory that tips due to a bifurcation in a parameter in (upper left), in (b) a trajectory that tips due to noise in the system (lower left), and in (c) a trajectory that is able to track a stable quasi-static equilibrium (upper right) until a critical rates at which point it tips away from the stable state (lower right).

to $\dot{x} = f(x, \lambda(t))$, but only when $\lambda(t)$ varies slowly enough [3]. We refer to the solutions of $f(x, \lambda(t)) = 0$ as stable or unstable *quasi-static equilibria* (QSE). Rate-induced tipping occurs when trajectories of the systems fail to track a stable QSE that is changing at a critical rate [2], or when $\lambda(t)$ changes faster than ‘slowly enough’. In essence, rate-tipping is about quantifying the boundary between slow changes that maintain the dynamics of the associated autonomous system and changes in parameters that are too fast.

update thisRate dependent tipping has been investigated using various well-developed mathematical theories, such as fast-slow theory [19, 24, 34] and pullback attractors [1]. Our approach is to investigate rate-tipping point phenomena using tools from nonautonomous bifurcation and stability theory.

1.2 Nonautonomous Stability

One method for understanding the stability of nonautonomous systems has been to investigate so-called attractor bifurcations which receive a thorough treatment in [29]. Much recent work on nonautonomous bifurcations focuses on determining the bifurcation structure of a solution by determining when stability of the corresponding linear variational equation changes under parameter variation [25, 26].

The general form of a nonautonomous ordinary differential equation depending on a parameter λ is

$$\dot{x} = f(x, t, \lambda) \quad (2)$$

for $x \in \mathbb{R}^n, t \in \mathbb{R}, \lambda \in \mathbb{R}^m$. Intuitively, a bifurcation of (2) is a qualitative change in the structure of solutions of (2) caused by a change in the parameter λ . In recent years, the theoretical foundations of bifurcation theory in nonautonomous systems has received considerable attention. Nonautonomous bifurcations and the related notion of attractivity in nonautonomous ordinary dynamical equations is investigated from a theoretical standpoint in [18, 20, 21]. Spectral theory and the stability theory for linear nonautonomous differential equations is used to investigate bifurcation and attractivity for nonautonomous differential equations in [30] and [27, 28]. The book [29] is an excellent reference for the bifurcation theory of nonautonomous differential equations.

The focus of many of these works (see e.g. [30]) is on determining when a solution or invariant set of (2) switches from being attracting to repelling (or vice versa) due to a variation in λ . For a nonautonomous linear equation $\dot{x} = A(t; \lambda)x$, the attractivity or repulsivity of the fixed point at the origin can be determined using one of a variety of stability spectra including the Lyapunov spectrum or exponential dichotomy spectrum [6, 10]. Let $x(t; x_0)$ denote the unique solution of (2) with initial condition x_0 . To determine the attractivity or repulsivity of $x(t; x_0)$ we pass to the associated linear variational equation

$$\dot{u}(t) = \frac{\partial f}{\partial x}(x(t; x_0), t, \lambda)u(t) \equiv A(t; \lambda)u(t) \quad (3)$$

Under mild hypotheses on $A(t; \lambda)$ and the nonlinear terms $f(x, t, \lambda) - A(t; \lambda)x$ the solution $x(t; x_0)$ is attracting or repelling whenever the fixed point at the origin of (15) is attracting or repelling. This serves as the theoretical basis for our methods.

In this paper we use Lyapunov exponents and their related QR approximation theory as our main tools to characterize stability. Lyapunov exponent theory provides a way of quantifying the repulsivity or attractivity of a time-dependent trajectory either in an asymptotic limit or along finite time-intervals. Since Lyapunov exponents are impossible to express exactly for most systems we approximate them using a time series of finite time Lyapunov exponents (FTLEs). Additionally we make use of Steklov averages which are quantities that give a measure of the local Lyapunov exponents of the system. The approximation of Lyapunov exponents and Steklov averages by QR methods makes use of the construction of an orthogonal change of variables to transform the linear variational equation to a time-dependent linear system with an upper triangular coefficient matrix. The columns of this change of variables define projections onto the stable and unstable Lyapunov vectors of a system and we use changes in the angles between the columns as an indication a change in the stable and unstable directions of the system.

The algorithms we use for the approximation of Lyapunov exponents by QR methods are given in Appendix A. In recent years the analysis of these methods [7, 11, 12, 14] and the related theory [13, 15] has received much attention. The idea behind QR methods is to compute the orthogonal factor in the QR factorization of a fundamental matrix solution of $\dot{u} = A(t)u$ (see equation (15)) to transform the original system to an upper triangular system from which the Lyapunov exponents can be approximated using the diagonal entries. Given a fundamental matrix solution $X(t)$ of (15) we can factor it uniquely as $X(t) = Q(t)R(t)$ where $Q(t)$ is orthogonal and $R(t)$ is upper triangular with positive diagonal entries. Under the change of variables $u(t) = Q(t)v(t)$, we obtain the resulting linear system $\dot{v} = B(t, \lambda)v(t)$ where the coefficient matrix $B(t, \lambda)$ is upper triangular [11]. Under the generic assumption that the system (15) is integrally separated or can be transformed to a block diagonal system with an integrally separated block structure, the Lyapunov exponents or Sacker-Sell spectrum are determined from the diagonal entries of $B(t)$ [13, 15]. For each $p \leq n$, the first p columns of the matrix $Q(t)$ form an orthogonal basis for the p Lyapunov vectors corresponding to the largest p Lyapunov exponents [8, 9]. Thus the columns of $Q(t)$ can be used to form orthogonal projections onto the stable and unstable subspaces of the system (15) and can also be useful in detecting non-autonomous bifurcation phenomena.

Efficient techniques (see e.g. [11, 12]) for computing $Q(t)$ avoid forming the fundamental matrix solution $X(t)$ and instead use only the coefficient matrix $A(t; \rho)$. The orthogonal factor $Q(t)$ can be shown to satisfy a system of n^2 differential equations which is preferable to solve rather than finding $X(t)$ since its global error is controlled entirely in terms of the local accuracy and is not restricted by numerical stability considerations

[12]. Additionally, $Q(t)$ remains bounded while $X(t)$ may become unbounded. This implies that the error in computing stability spectra and related quantities can be controlled in terms of the local accuracy and is robust even in the presence of unbounded solutions.

1.3 Model Problems and the compost bomb instability

In this paper we view rate-induced tipping through the lens of nonautonomous stability theory. We find that this is a quantitative method to verify a qualitative change that is often identified using the “eyeball test” - where one physically sees the graph of the system tip. Not only does this method provide a threshold to measure tipping, it also gives a rate of separation away from the stable QSE. **Do we talk about this later?** In Appendix A we delineate the algorithm used to compute relevant spectral quantities and in the following sections we explore different model problems using nonautonomous stability theory. In Sections 2 and 3, we consider model problems in the framework of (2) of the form

$$\dot{x} = f(x, \lambda(at))$$

for $x \in \mathbb{R}^n, \lambda \in \mathbb{R}^m$ where λ depends on some real parameter a that defines its growth or decay rate. We will consider two model problems: one with a unique stable QSE,

$$\dot{x} = -(x - \lambda(t))(x - \lambda(t) - \delta), \quad (4)$$

and one that is bistable for any fixed λ ,

$$\dot{x} = -(x - \lambda(t))(x - \lambda(t) - \delta)(x - \lambda(t) + \delta). \quad (5)$$

Each model problem will be examined under two different types of parameter drift as seen in Section 2 and Section 3. We start by verifying our method detects tipping for problems with asymptotically constant parameter drift, like those studied by Ashwin, Perryman, and Wieczorek [1]. We then consider problems where the methods in [1] fail, in particular systems with *linear ramping*, where the parameter increases at a constant rate. This leads to the example of the “compost bomb instability,” where the tipping mechanism is linear ramping.

In Section 4 we demonstrate connections between indicators of nonautonomous stability and rate-induced tipping in the “compost bomb instability.” The compost bomb instability [34] is a hypothetical climate phenomenon in which global warming causes the peatlands to catch fire, as hypothesized in various climate papers [4, 16, 17]. The burning peat releases more carbon into the atmosphere creating a positive feedback. The equations for the compost bomb are

$$\begin{aligned} \epsilon \dot{T} &= Cre^{\alpha T} - \frac{\lambda}{A}(T - T_a) \\ \dot{C} &= \Pi - Cre^{\alpha T} \\ \dot{T}_a &= v, \end{aligned} \quad (6)$$

where T is soil temperature, C is soil carbon content, and T_a is the atmospheric temperature [4, 34]. Soil carbon is increased by litter fall from plants (Π) and decreased by microbial decomposition ($Cre^{\alpha T}$). Global warming is included by assuming that T_a increases at a constant rate v (in $^{\circ}\text{C yr}^{-1}$). Wieczorek et al. [34] show that the critical factor in setting off the compost bomb instability is the rate of warming, v , as opposed to a particular atmospheric temperature T_a . With the parameters values listed in Table 1, any fixed value T_a (i.e., $v = 0$) will lead to an attracting equilibrium state. If T_a increases due to slow, linear ramping, the system remains near the QSE for all time. However, if the ramping rate is increased above a critical value, the compost bomb instability is triggered, and the soil temperature warms by an order of magnitude over the course of a few decades.

For each of the examples above, we use Matlab and what ODE solver? to numerically solve the systems for different parameter values, and numerically approximate the tipping value. We also use the algorithm in Appendix A to calculate and plot the time series for the FTLE and Steklov averages as well as computing a time-series of the angle between the finite-time Lyapunov vectors corresponding to different parameter values. We see that the numerical methods indicate tipping for all examples.

Parameter	Value	Unit	Parameter	Value	Unit
r	0.01	yr ⁻¹	α	$\frac{\ln(2.5)}{10}$	°C ⁻¹
λ	5.049×10^6	J yr ⁻¹ m ⁻² °C ⁻¹	A	3.9×10^7	J kg ⁻¹
Π	1.055	kg m ⁻² yr ⁻¹	ϵ	0.064	kg m ⁻² °C ⁻¹

Table 1: Parameters used by Wiezcorek et al. [34] in analyzing the “compost bomb instability.”

Sections 2 and 3 contain this analysis for the model problems given above with different kinds of parameter functions. We see that Section 2 also contains analytical results showing the existence of a heteroclinic orbit to support our analysis of the rate-tipping in the case of asymptotically constant parameter drift. Section 4 contains our analysis of the compost bomb problem, and Section 5 contains a discussion of the results.

2 Examples: Asymptotically Constant Parameter Drift

Rate-induced tipping can be shown, analytically in some examples, through a heteroclinic connection in an extended system. In this section, we show that the heteroclinic connection occurs for the same parameter value as a nonautonomous bifurcation. In Section 2.1 we consider a system with a unique QSE. For this example we find the heteroclinic connection and show that it is unique using a Melnikov integral calculation (for the Melnikov integral calculation, see Appendix B). We then show that when we consider the same system in the nonautonomous framework, we get a bifurcation for the same parameter value using finite time Lyapunov exponents and Steklov averages. In Section 2.2 we consider a system with two stable QSEs and do a similar analysis.

2.1 Example with a unique QSE and asymptotically constant parameter drift

We consider the system

$$\dot{x}(t) = -(x(t) - \lambda(t))(x(t) - \lambda(t) - \delta) \quad (7)$$

where $\lambda(t)$ satisfies the logisitic differential equation

$$\dot{\lambda}(t) = a\lambda(t)(1 - \lambda(t)) \quad (8)$$

with parameter $a > 0$. Notice that since the $\dot{\lambda}$ equation doesn’t depend on x , we can solve for λ directly, given initial conditions. In fact we have

$$\lambda(t) = \frac{e^{at}}{\lambda_1 + e^{at}}$$

where

$$\lambda_1 = \frac{1 - \lambda_0}{\lambda_0}$$

and λ_0 is the initial condition on λ . In this example we take $\delta = 0.5$, $\lambda_0 = 10^{-6}$, and $x_0 = 0.5$. Note that the following analysis is valid for $\delta \in (0, 1)$ with the stipulation that tipping point in the parameter a is dependent on the choice of δ .

In Figure 2 we see the behavior of the system for different values of a (Figure 2 (a), (b), and (c)) and the corresponding stability spectra of Lyapunov exponents and Steklov averages as functions of time (Figure 2 (d) and (e)). In Figure 2(a), we have that $a = .4999$ and we see that the trajectory (black curve) tracks the stable QSE (red dashed curve) until about $t = 25$, tracks the unstable QSE (blue dashed curve) for $t = 25$ to $t = 40$, then is attracted back to the stable QSE at $t = 40$, becoming exponentially close by $t = 60$. In Figure 2(b), $a = .5$ and the trajectory tracks the stable QSE until $t = 25$ then tracks the unstable QSE. The trajectory will continue to track the unstable QSE fro $t > 25$. This phenomenon that we see in Figure 2(b) is analogous to a heteroclinic connection (further discussion of this follows below). In Figure 2(c), $a = .5001$

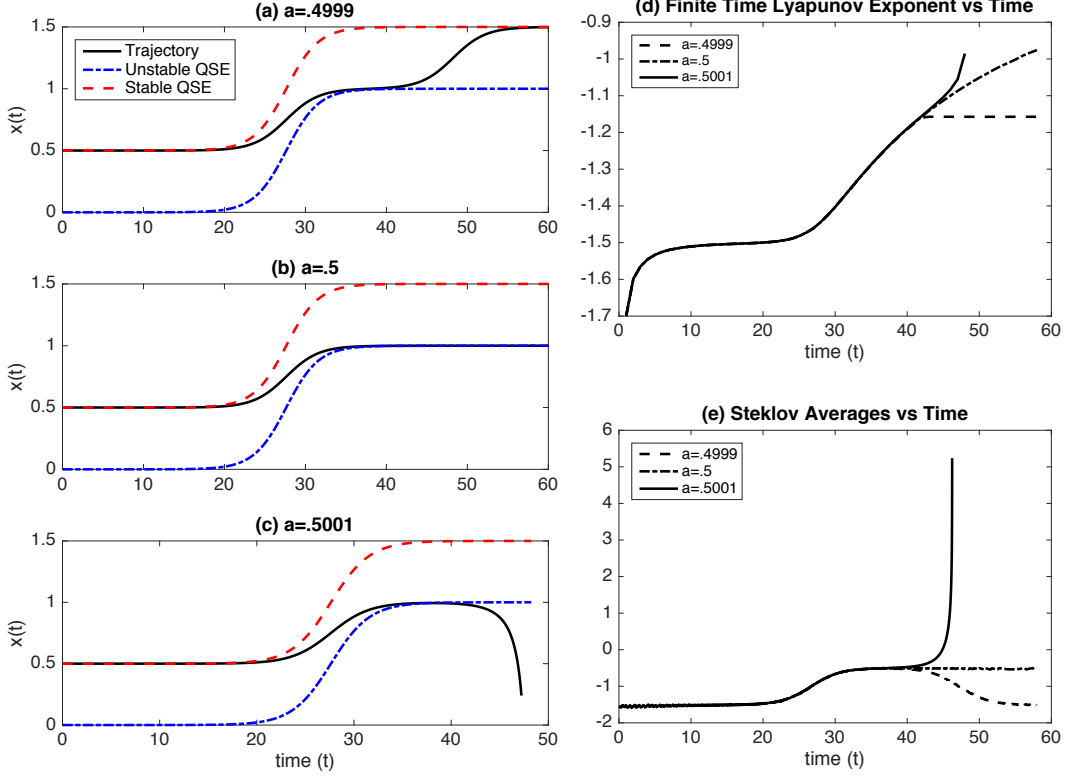


Figure 2: Rate tipping in a system with a unique stable QSE under asymptotically constant parameter growth. On the left we have trajectories (black) for different rates, a . On the right we have the stability spectra for the trajectories under consideration. See text for a detailed description.

and the trajectory tracks the stable QSE until $t = 25$, the unstable QSE from $t = 25$ to $t = 38$, then crosses over the unstable QSE and diverges to negative infinity at $t = 38$. These three figures together show us, using the “eyeball test,” that the tipping point for the system is near $a = .5$.

We can confirm that $a = 0.5$ is a tipping point of Equation 7 using nonautonomous bifurcation theory. Here we compute the Lyapunov exponents and Steklov averages of window length $H = 2$ as a function of time as described in Appendix A and plot the results in Figure 2 (d) and (e). In Figure 2(e), when $t = 0$, the Steklov averages of window length two is -1.5 for all values of a . Furthermore for the trajectory with $a = .4999$, the sequence of Steklov averages limit to -1.5 as $t \rightarrow \infty$ with a deviation towards 0 between $t = 20$ and $t = 50$ indicating that the trajectory moved away from the stable QSE but was eventually pulled back as we saw in Figure 2(a). Notice that as $a \rightarrow .5$ but with $a < .5$ we would see this time window increase as the trajectory spends more time near the unstable QSE. Indeed in Figure 2(e) for the trajectory with $a = .5$ the Steklov average plot appears as a step-like function where the plot starts at -1.5 , jumps up to -0.5 and remains at -0.5 for all time. This occurs because for $a = .5$ we have heteroclinic connection in the extended system where λ is a state variable instead of a parameter. For $a > .5$, the Steklov average plot diverges to positive infinity. This clear behavior confirms the tipping behavior shown in our earlier analysis.

For this model problem, we can analytically find the tipping value to be $a = 0.5$ by finding a heteroclinic orbit connection between two equilibrium points. The system of differential equations given by (7) and (8) has four equilibria, located at $(0, 0)$, $(\delta, 0)$, $(1, 1)$, and $(1 + \delta, 1)$. The heteroclinic orbit is the connection between the unstable subspace of the equilibrium point $(\delta, 0)$ and the stable subspace of $(1, 1)$. Phase portraits for the extended system for different values of a are given in Figure 3. The middle figure of Figure 3 shows the existence of the heteroclinic connection indicated by the black line connecting the equilibrium at $(.5, 0)$ to the equilibrium at $(1, 1)$. For analytical confirmation that this heteroclinic connection exists and is unique, please refer to Appendix B.

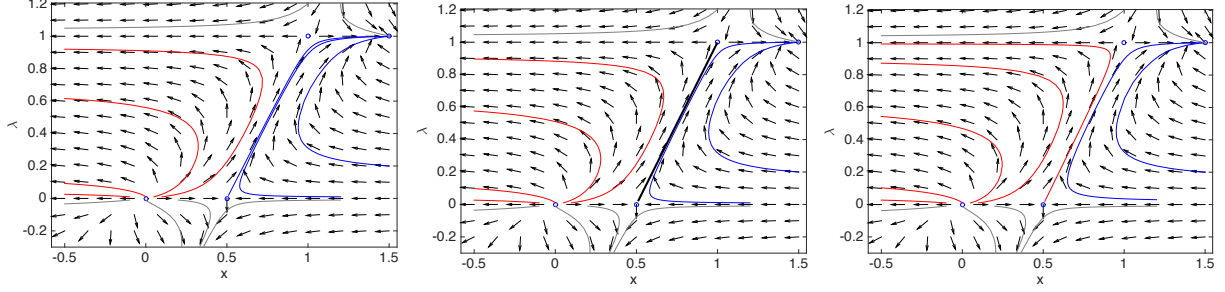


Figure 3: Phase portraits of extended system for $a < 0.5$ (left), $a = 0.5$ (middle), and $a > 0.5$ (right). We can see the existence of a heteroclinic orbit at $a = 0.5$ by the black trajectory that connects the equilibrium at $(.5, 0)$ to the equilibrium at $(1, 1)$. In each figure, blue trajectories converge to the stable equilibrium at $(1.5, 1)$ and red trajectories have x tending to negative infinity.

2.2 Example with bistability and asymptotically constant parameter drift

The above example has only one stable QSE. In the following example we consider a bistable case with asymptotically constant parameter drift. The system is

$$\dot{x}(t) = -(x(t) - \lambda(t))(x(t) - \lambda(t) - \delta)(x(t) - \lambda(t) + \delta) \quad (9)$$

where $\lambda(t)$ satisfies Equation 8 and as in the previous example, we take $\delta = 0.5$, $\lambda_0 = 10^{-6}$, and $x_0 = 0.5$. The system behaves in much the same way as the example from Section 2.1. In Figure 4(a-c) we see plots of the solution $x(t, x_0)$ generated from different values for a . Notice that the system tips to the bottom stable QSE at $t = 45$ in 4(c), which corresponds to a tipping value of $a \approx 0.377$. This occurs because of a heteroclinic bifurcation which can be shown in the same way as in the previous model problem.

In the bistable case we find that an extended system must be analyzed to understand the stability of the original system due to the fact that when the system “tips” it does not diverge as it did in the case with the unique stable QSE, but instead tracks a different stable QSE. Due to this phenomenon of tracking a different stable QSE, it is nontrivial to show the tipping point in the bistable case with the nonautonomous theory because the stability spectra do not detect a divergence to plus or minus infinity. The analysis conducted in Section ?? is not sufficient to determine the tipping point because it is possible to have identical FTLE and Steklov averages plots for tipped and untipped trajectories as can be seen in 4(d) and (e). A trajectory that tracks the unstable QSE for a particular length of time may either return to tracking the original QSE or tip and begin tracking the other QSE, depending if the value of a is less or greater than the tipping point. We see this phenomenon in Figure 4(e) namely that the Steklov average (of window length $H = 2$) versus time is the same for $a = 0.376$ and $a = 0.378$, but $a = 0.376$ corresponds to a trajectory that tracks the original stable QSE and $a = 0.378$ corresponds to a trajectory that tracks the other stable QSE!

In particular, trying to use nonautonomous theory is tricky in a one-dimensional system because either $Q(t) = 1$ or $Q(t) = -1$ (in the QR decomposition, see Appendix ??), which does not admit the possibility of using $Q(t)$ to determine directions of growth and decay. For this reason we introduce an extended system

$$\begin{aligned} \dot{x}(t) &= -(x(t) - \lambda(t))(x(t) - \lambda(t) - \delta)(x(t) - \lambda(t) + \delta) \\ \dot{y}(t) &= \frac{1}{2}x^2(t) - y(t) \end{aligned} \quad (10)$$

where $\lambda(t)$ satisfies the same differential equation (Equation 8) with parameter values $\delta = 0.5$, $\lambda_0 = 10^{-6}$, and $x_0 = 0.5$. In Equation 10, the x variable is uncoupled with the y variable and therefore the dynamics in x are unchanged. However, the addition of the y variable means that $Q(t)$ is now a nonconstant 2×2 matrix and the columns of $Q(t)$ can be monitored to detect changes in stability.

In Figure 4(f), we monitor the angle between the first columns (the columns that correspond to the x variable) of different $Q(t)$ matrices vs. time. The dashed plot shows the angle between the first column of $Q(t)$ when $a = .376$ (call it $Q_1(t)$) and the first column of $Q(t)$ when $a = .377$ (call it $Q_2(t)$). Notice that the plot starts off near zero, moves away around $t = 50$ up to a value of .45 at around $t = 70$, then

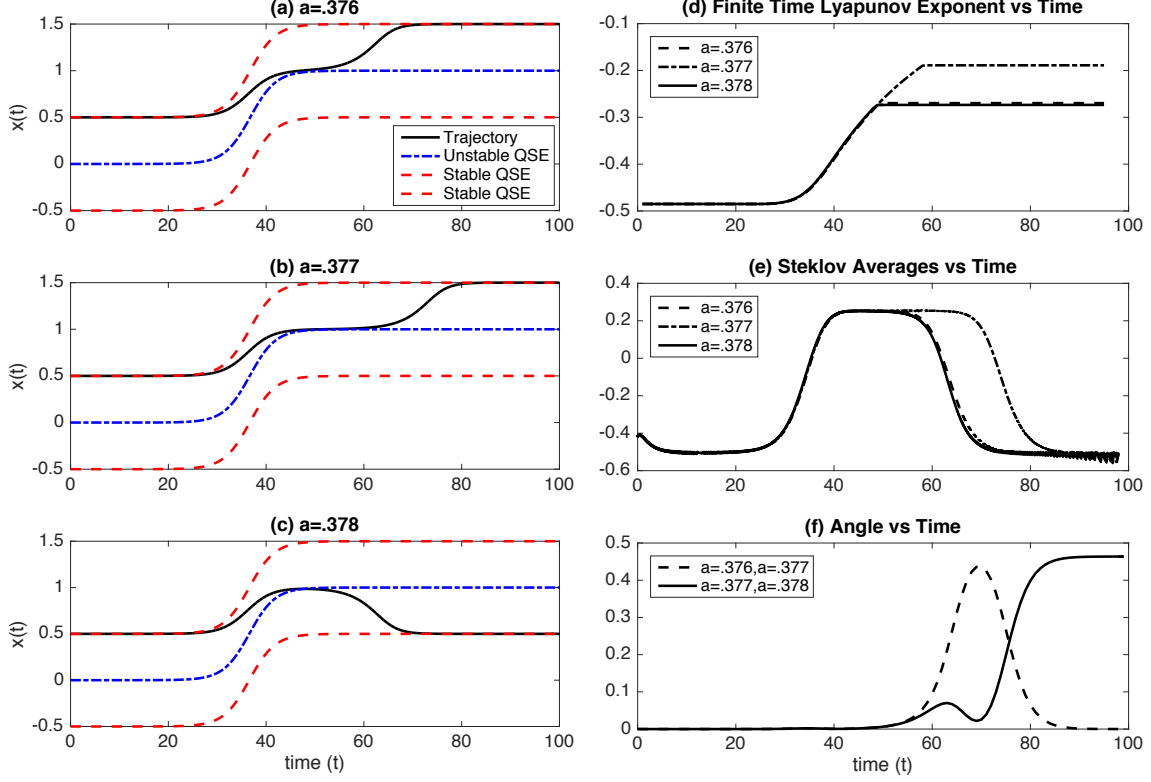


Figure 4: Rate tipping in a system with two stable QSEs under asymptotically constant parameter growth. On the left we have trajectories (black) for different rates, a . On the right we have the stability spectra for the trajectories under consideration. See text for detailed description.

returns to zero. This indicates that the trajectories initially followed the same path (when the angle was zero), tracked different paths for a time, and then tracked the same path (when the angle returned back to zero). Conversely, the solid plot is the angle between the first column of $Q_2(t)$ and the first column of $Q(t)$ when $a = .378$ (call it $Q_3(t)$). Notice that again the plot starts at zero, but after it moves away around $t = 50$, never returns back to zero, instead staying at a value of about .45 for $t > 85$. This tells us that the trajectory is tracking a different stable QSE, i.e. that the system has tipped. In this way we are able to detect the “tipping” point of $a \approx 0.377$.

Because the parameter λ is asymptotically constant, we can analytically find the tipping value to be $a \approx 0.377$ by finding a heteroclinic orbit connection between two equilibrium points. In Figure 5 we see the phase portraits for the system of differential equations given by (9) and (8). This system has six equilibria, located at $(-\delta, 0)$, $(0, 0)$, $(\delta, 0)$, $(1 - \delta, 1)$, $(1, 1)$, and $(1 + \delta, 1)$. The heteroclinic orbit is the connection between the unstable subspace of the equilibrium point $(\delta, 0)$ and the stable subspace of $(1, 1)$. Phase portraits for different values of a are given in Figure 5. In the middle plot of Figure 5, we see the existence of the heteroclinic connection indicated by the black line connecting the equilibrium at $(.5, 0)$ to the equilibrium at $(1, 1)$. For analytical confirmation that this heteroclinic connection exists and is unique, please refer to Appendix B.

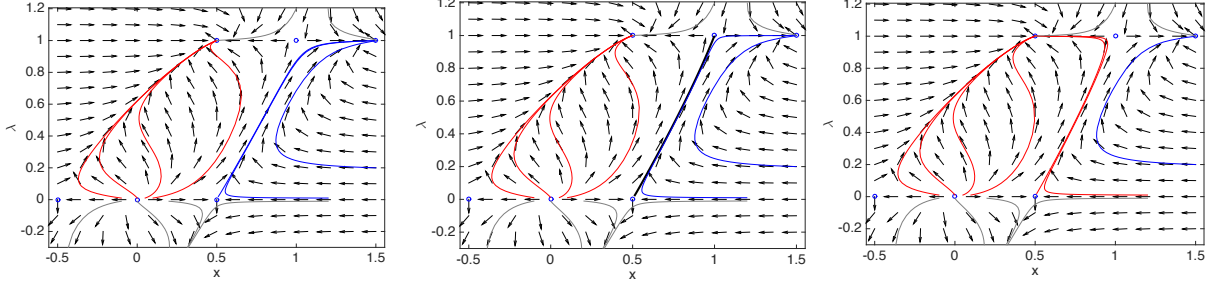


Figure 5: Phase portraits of extended system for $a < 0.377$ (left), $a = 0.377$ (middle), and $a > 0.377$ (right). We can see the existence of a heteroclinic orbit at $a = 0.377$ by the black trajectory that connects the equilibrium at $(.5, 0)$ to the equilibrium at $(1, 1)$. In each figure, blue trajectories converge to the stable equilibrium at $(1.5, 1)$ and red trajectories converge to the stable equilibrium at $(.5, 1)$.

3 Examples: Constant Parameter Ramping

When λ increases at a constant rate, the extended system has no equilibrium points, precluding the possibility of a heteroclinic connection. However, the same qualitative behavior relative to the QSE is observed. In this section, we show numerically that the system exhibits rate-induced tipping for the same parameter value as a nonautonomous bifurcation.

3.1 Example with a unique QSE and constant parameter ramping

Consider the system

$$\begin{aligned}\dot{x} &= -(x - \lambda)(x - \lambda - \delta) \\ \dot{\lambda} &= a\end{aligned}\tag{11}$$

This system, like the example in (7), contains a stable and an unstable QSE which are a constant distance δ apart. However, in this system λ increases at a constant rate, an affect known as *parameter ramping*, which causes all solutions of this system to be unbounded. In this example we take $\delta = 0.5$, $\lambda_0 = 10^{-6}$, and $x_0 = 0.5$. The first three subfigures of Figure 6 show the solution $x(t, x_0)$ generated from different values for a . In Figure 6(a) the example trajectory tracks the stable QSE $x(t) = at + \delta$. Here a is smaller than the tipping value. In Figure 6(c), corresponding to $a = 0.065$, we see that the system tips, i.e. $x(t, x_0)$ diverges from the stable QSE to the unstable QSE $x(t) = at$, around time $t = 58$.

We can compare this observation of tipping to numerical calculations of FTLE and Steklov averages of window length $H = 2$ in Figures 6(d), 6(e). Figure 6(e) shows the Steklov averages for trajectories before and after tipping. Note that for the trajectory before the tip, the Steklov averages level off as the trajectory settles into a path tracking the stable QSE, while for the trajectory with tipping, the Steklov averages blow up at the same time as the trajectory tips.

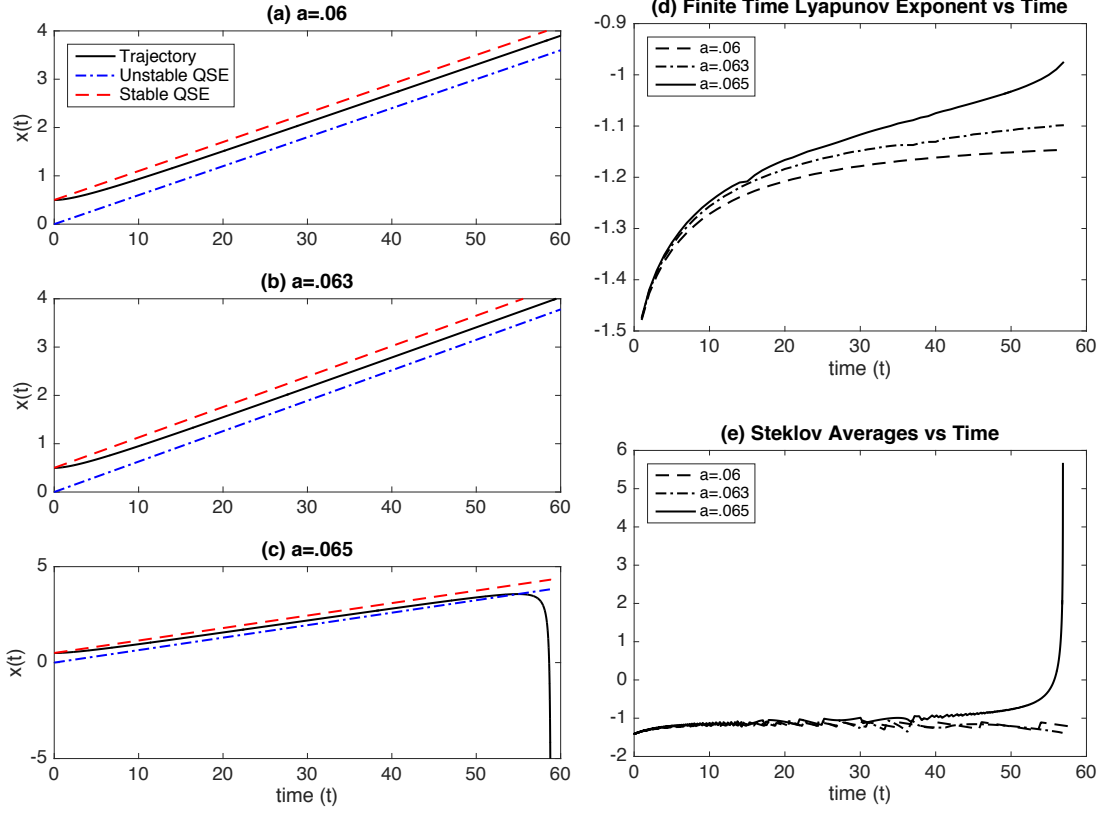


Figure 6: Rate tipping in a system with a unique stable QSE under linear parameter growth. On the left we have trajectories (black) for different rates, a . On the right we have the stability spectra for the trajectories under consideration. See text for a detailed description.

3.2 Example with bistability and constant parameter ramping

Here we consider a system with two stable QSE and one unstable QSE. In this example, as in the previous example, solutions and QSE are still unbounded, but the tipping does not lead to escape in an opposite direction; the system tips by moving past the unstable QSE and then tracks a different stable QSE (similar to the example in Section 2.2). The equations we use for this example are:

$$\begin{aligned}\dot{x} &= -(x - \lambda)(x - \lambda - \delta)(x - \lambda + \delta) \\ \dot{\lambda} &= a\end{aligned}\tag{12}$$

The two stable QSE are $x(t) = at \pm \delta$ and the unstable is $x(t) = at$ with $\delta = .5$. Again, we consider a trajectory given by $\lambda_0 = 10^{-6}$, and $x_0 = 0.5$. In Figure 7(a,b), we see examples where the ramping parameter a is small enough to not cause tipping. The trajectory tracks a stable QSE. In Figure 7(c), the ramping parameter is $a = 0.049$ and the system tips at $t = 105$. We are able to conclude that tipping happens at $a \approx 0.049$.

Figures 7(e) and 7(d) show how tipping and tracking a different QSE are indicated by Steklov averages of window length $H = 2$ and FTLE, respectively. For a non-tipping trajectory, the Steklov averages are negative. When there is tipping, we see the Steklov averages have a positive peak at the same time as tipping, and then drops to a negative value and levels as the trajectory tracks one of the stable QSE.

Again in this bistable QSE example, we find that an extended system must be analyzed to understand the stability of the original system. We introduce an extended system

$$\begin{aligned}\dot{x}(t) &= -(x(t) - \lambda(t))(x(t) - \lambda(t) - \delta)(x(t) - \lambda(t) + \delta) \\ \dot{y}(t) &= x(t) - y(t)\end{aligned}\tag{13}$$

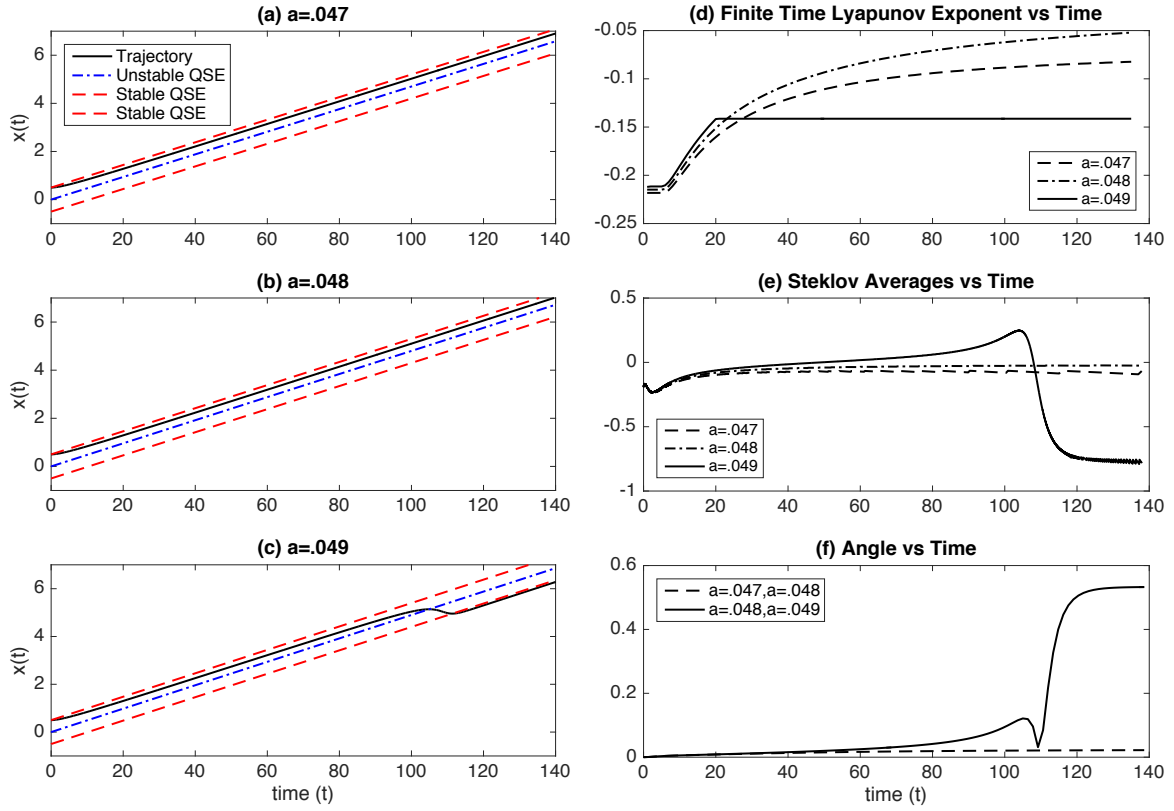


Figure 7: Rate tipping in a system with a two stable QSEs under linear parameter growth. On the left we have trajectories (black) for different rates, a . On the right we have the stability spectra for the trajectories under consideration. See text for a detailed description.

where $\lambda(t)$ satisfies the same differential equation (Equation 8) with parameter values $\delta = 0.5$, $\lambda_0 = 10^{-6}$, and $x_0 = 0.5$. In Equation 13, the x variable is again uncoupled with the y variable and therefore the dynamics in x are unchanged.

In Figure 7(f), we monitor the angle between the first columns (the columns that correspond to the x variable) of different $Q(t)$ matrices vs. time. The dashed plot shows the angle between the first column of $Q(t)$ when $a = .047$ (call it $Q_1(t)$) and the first column of $Q(t)$ when $a = .048$ (call it $Q_2(t)$). Notice that the plot starts off near zero, and continually moves slightly away from zero, but stays very small. This behavior indicates that the trajectories follow very similar paths because the angle is close to zero. Due to the fact that λ has constant parameter ramping, the trajectories for different values of a will track the stable QSE at different distances, even if the trajectory doesn't tip to the other stable QSE. For this reason, the angle between two untipped trajectories will be small but nonzero.

In Figure 7(f), the solid plot is the angle between the first column of $Q_2(t)$ and the first column of $Q(t)$ when $a = .049$ (call it $Q_3(t)$). Notice that again the plot starts at zero, but after it moves away around $t = 50$, never returns back to zero, instead staying at a value of about .5 for $t > 120$. This tells us that the trajectory is tracking a different stable QSE, i.e. that the system has tipped. In this way we are able to detect the “tipping” point of $a \approx 0.048$.

4 Compost Bomb

In this section we re-examine the compost bomb instability [34] using the algorithms we have developed and test. The goal here is to extend the results of [34] away from the singular limit where the geometric intuition may no longer apply. In so doing we show that our methods can be in the same context as the current theoretical techniques and in problems where these techniques can not be applied. This is especially relevant for applications in climate science where most realistic modeling is done using computers.

Because Wieczorek et al., focused on the singular limit (i.e., $\varepsilon = 0$) of a singularly perturbed system, they were able to find an $\mathcal{O}(\varepsilon)$ approximation for the tipping rate. They appended a differential equation for the time-dependent parameter (T_a) to create a system with 1 fast variable (soil temperature, T) and 2 slow variables (soil carbon concentration C and atmospheric temperature under global warming T_a). The regime with $v = 0$ corresponds to no global warming, and it is the only regime in which the compost bomb system (6) contains an equilibrium point. In this regime, T_a remains constant and the equilibrium is stable for all values of T_a assuming the other parameters take the values listed in Table 1. Thus, v becomes the critical rate that causes the system to tip above a certain threshold.

Wieczorek et al. show that the critical rate for v corresponds to a canard trajectory—that is, a trajectory that crosses from a stable slow manifold to unstable slow manifold [33]—in the singular limit. In the compost bomb system, a canard arises due to a folded saddle point. Folded equilibria, including folded saddles, are special singularities that arise in singularly perturbed systems with folded critical manifolds that indicate a change in orientation of the slow flow with respect to fold. Because of their connection with canard trajectories, folded singularities are associated with complicated and interesting dynamical phenomena. Much of the discussion of folded equilibria is beyond the scope of this paper, but further reading on folded saddles (and folded singularities in general) can be found in [5, 32].

Each folded saddle in a 1-fast, 2-slow system comes equipped with exactly one true canard trajectory and one ‘faux canard’ trajectory that passes from an unstable slow manifold to a stable slow manifold. In the singular limit, the dynamics on the stable slow manifold near the folded saddle are indistinguishable from a typical saddle. That is, the folded saddle comes equipped with its own 1D stable and unstable manifolds that are contained within the 2D slow manifold. The stable manifold to the folded saddle is the canard trajectory and the unstable manifold is the faux canard. Also like a traditional saddle, the stable manifold to a folded saddle separates points that have vastly different dynamics in the long run. On one side of the stable manifold to the folded saddle, trajectories are blocked from reaching the fold by the faux canard. In terms of the compost bomb, these trajectories remain near the original QSE and thus exhibit tracking behavior. On the other side of the stable manifold to the folded saddle, trajectories reach the fold and take a large excursion away from the fold. In terms of the compost bomb, these trajectories are said to have tipped.

In [34], Weiczorek et al. fix an initial condition that corresponds to the QSE. For small values of v , the

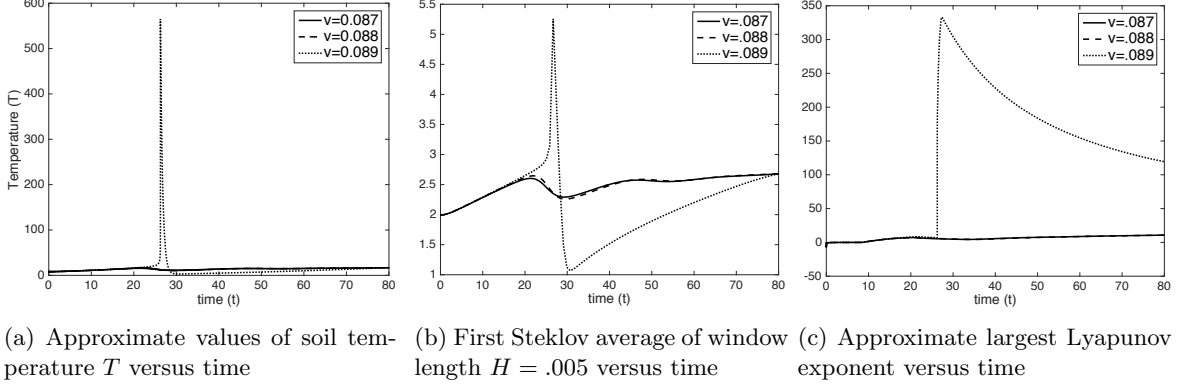


Figure 8: Rate tipping in the Compost Bomb Instability [34] with $\epsilon \approx 0.064$ and initial condition $(8.15, 50, 0)^T$. We have (a) plots of the trajectory in phase space, (b) first Steklov average of window length $H = .005$, and (c) the approximate largest Lyapunov exponents.

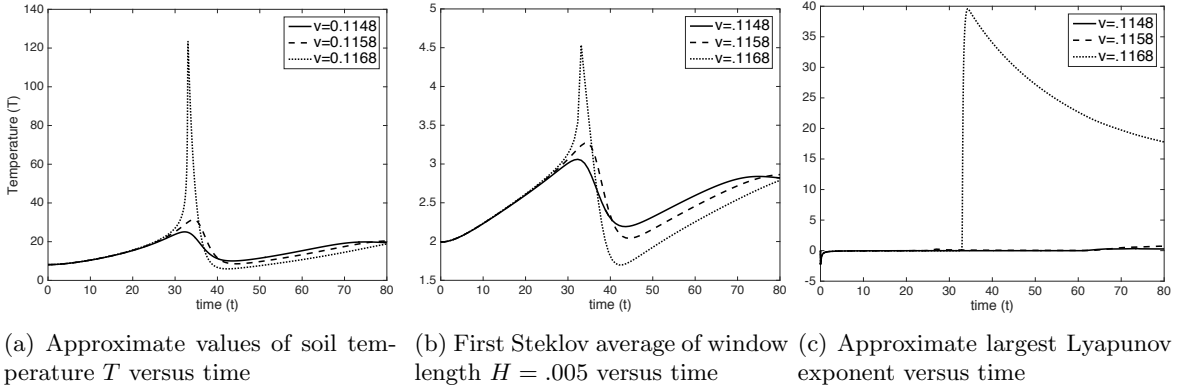


Figure 9: Rate tipping in the Compost Bomb Instability [34] with $\epsilon = 0.2$ (away from the singular limit) and initial condition $(8.15, 50, 0)^T$. We have (a) plots of the trajectory in phase space, (b) first Steklov average of window length $H = .005$, and (c) the approximate largest Lyapunov exponents.

initial condition lies in the region that is bounded away from the fold. As v is increased, the stable manifold to the folded saddle moves and eventually passes through the initial condition, so that for high enough values of v the initial condition lies on a trajectory that takes a large excursion. Then the tipping point (for $\epsilon = 0$) is precisely the value of v where the initial condition lies on the stable manifold to the folded saddle. It is a global bifurcation akin to a heteroclinic connection, but this interpretation relies on the ability to treat the system as a singular perturbation problem.

The excitability of the system (6) is investigated in [34] using the parameter value $\epsilon \approx 0.064$ which was chosen so that $\epsilon = \mu/A$ where $\mu = 2.5 \times 10^6$ is the thermal inertial of the soil. As the parameter v in (6) varies increases from 0.8 to 0.9, the system exhibits a "single-spike excitable response" for the initial condition $(8.15, 50, 0)^T$ and has a tipping point at $v \approx 0.09$ in the sense that soil temperature T spikes above the critical threshold of 100° Celsius. In Figure 8 we use our algorithm to approximate the that for v in the interval $[0.086, 0.089]$, there is a sudden change in the first Steklov average for $H = 0.005$ and the approximate largest Lyapunov exponent at $v = 0.089$. If desired, one could use a bisection-type method to more precisely estimate the smallest value of v at which the system tips.

In Figure 9 we investigate tipping phenomena of (6) using a value of $\epsilon = 0.2$ which corresponds to a higher value of $\mu = 7.8e6$ for the thermal inertial of soil or a smaller value of A . As v transitions from 0.1148 to 0.1168 we a similar, although less drastic, spike in the soil temperature that occurs at a later time than that for the value of $\epsilon = 0.064$ using the same initial condition of $(8.15, 50, 0)^T$. This shows that we can apply our methods when $\epsilon = 0.2$ is further from the singular limit.

5 Discussion

Goal was to use technique for higher dimensional systems, but we don't have an example. Added to discussion: We think this will be effective in higher dimensional systems because of the whole angle between trajectories thing

By exploring a connection between rate-induced tipping and nonautonomous bifurcations, we have developed a numerical method for detecting rate-induced tipping points. Except for one-dimensional systems with asymptotic parameter drift, the primary method of detecting rate-induced has been the “eyeball test”—that is, simulating a system for ‘long enough’ time to plot a solution and observe tipping. The trouble with the eyeball test is that for the precise rate where tipping occurs, the solution could track an unstable QSE indefinitely. Figure 4 gives some indication of this phenomenon. Indeed, the behavior of tracking an unstable QSE is not surprising given that a canard trajectory plays an integral role in the compost bomb phenomenon [34].

In their analysis, Wieczorek et al. analytically demonstrate rate-tipping in the compost bomb by proving the existence of a heteroclinic-type connection on the critical manifold of a singularly perturbed system. The connection occurs when an initial condition lies on the stable manifold to a folded saddle equilibrium, which is the unique singular canard trajectory. The behavior of tracking an unstable QSE for an extended period of time, especially in systems with two stable QSEs, is reminiscent of canard behavior in quintessential example of canard orbits, the Van der Pol system. While tracking the QSE, there is no way to know if the system will return to the stable QSE corresponding to the initial conditions or jump across to the other stable QSE (see Figures 4 and 7).

This connection with canards illustrates issues with the eyeball test beyond lack of rigor. It also highlights the pitfalls of only using Steklov averages or FTLEs to detect rate-induced tipping points when viewed as nonautonomous bifurcations in systems exhibiting bistability. Steklov averages and FTLEs only indicate that a system is tracking a stable QSE, but not which QSE. In bistable systems, Steklov averages and FTLEs can provide evidence in support of tipping in conjunction with simulated trajectories, but they cannot fully determine whether or not a system has tipped. However, a change in sign of the Steklov averages or FTLEs in conjunction with a change in the angle corresponding to the leading FTLE is enough to numerically demonstrate rate-tipping.

We have only demonstrated this connection for low-dimensional systems, however it is worth noting that the technique is perhaps better suited for higher dimensional systems. Because the angle of the leading FTLE is continuous in time, the algorithm requires a system with at least two state variables (not including an appended equation for the time-dependent parameter). We believe the work presented here is just the start, with many opportunities for further exploration.

Acknowledgments

The authors would like to thank Mary Silber and Eric Van Vleck for their guidance throughout this project. We also thank Sebastian Wieczorek for his suggestion to consider problems with two stable QSEs. This material is based upon work supported by the AMS Mathematics Research Communities (National Science Foundation Grant No. 1321794) and the Mathematics and Climate Research Network (NSF Grants DMS-0940366 and DMS-0940363).

References

- [1] P. Ashwin, C. Perryman, and S. Wieczorek, Parameter shifts for nonautonomous systems in low dimension: Bifurcation and rate-induced tipping, arXiv preprint arXiv:1506.07734 (2015).
- [2] ———, S. Wieczorek, R. Vitolo, and P. Cox, Tipping points in open systems: bifurcation, noise-induced and rate-dependent examples in the climate system, Philosophical Transactions of the Royal Society of London A: Mathematical, Physical and Engineering Sciences **370** (2012), no. 1962, 1166–1184.
- [3] S. Baer, T. Erneux and J. Rinzel, The Slow Passage Through a Hopf Bifurcation: Delay, Memory Effects, and Resonance, SIAM Journal on Applied Mathematics **49(1)** (1989), 55–71.

- [4] P. Cox, R. Betts, C. Jones, S. Spall, and I. Totterdell, Acceleration of global warming due to carbon-cycle feedbacks in a coupled climate model, *Nature* **408** (2000), no. 6809, 184–187.
- [5] M. Desroches, J. Guckenheimer, B. Krauskopf, C. Kuehn, H. Osinga, and M. Wechselberger, Mixed-mode oscillations with multiple time scales, *SIAM Review* **54** (2012), no. 2, 211–288.
- [6] L Dieci and E.S. Van Vleck, Lyapunov and other spectra: a survey, *Collected lectures on the preservation of stability under discretization* **109** (2002), 197.
- [7] L. Dieci and Van Vleck, E.S., On the error in QR integration, *SIAM J. Numer. Anal.* **46**, no **3**. (2009), pp 1166–1189.
- [8] L. Dieci, Van Vleck, E.S., and Elia, C., Exponential dichotomy on the real line: Svd and qr methods, *J. Diff. Eqn.* **248** (2010), pp 287–308.
- [9] ———, Detecting exponential dichotomy on the real line: SVD and QR algorithms, *BIT* **51** (2011), pp 555–579.
- [10] Luca Dieci and Erik S Van Vleck, Lyapunov and sacker–sell spectral intervals, *Journal of dynamics and differential equations* **19** (2007), no. 2, 265–293.
- [11] Dieci, L. and Van Vleck, E.S., Computations of orthonormal factors for fundamental solution matrices, *Numer. Math.* **83** (1990), pp. 599–620.
- [12] ———, Unitary integrators and applications to continuous orthonormalization techniques, *SIAM J. Numer. Anal.* **310** (1994), pp. 261–281.
- [13] ———, Lyapunov spectral intervals: Theory and computation, *SIAM J. Numer. Anal.* **40** (2003), pp. 516–542.
- [14] ———, On the error in computing Lyapunov exponents by QR methods, *Numer. Math.* **101** (2005), pp. 619–642.
- [15] ———, Lyapunov and Sacker-Sell spectral intervals, *J. Dyn. Diff. Eqn.* **19** (2007), pp. 263–295.
- [16] DV Khvorostyanov, G Krinner, P Ciais, M Heimann, and SA Zimov, Vulnerability of permafrost carbon to global warming. part i: model description and role of heat generated by organic matter decomposition, *Tellus B* **60** (2008), no. 2, 250–264.
- [17] DV Khvorostyanov, Philippe Ciais, Gerhard Krinner, SA Zimov, Ch Corradi, and Georg Guggenberger, Vulnerability of permafrost carbon to global warming. part ii: sensitivity of permafrost carbon stock to global warming, *Tellus B* **60** (2008), no. 2, 265–275.
- [18] P.E. Kloeden and S. Siegmund, Bifurcations and continuous transitions of attractors in autonomous and nonautonomous systems, *International J. Bifurcation and Chaos* **15(3)** (2005), 743–762.
- [19] C. Kuehn, A mathematical framework for critical transitions: bifurcations, fast-slow systems and stochastic dynamics, *Physica D: Nonlinear Phenomena* **240(12)** (2011), 1020–1035.
- [20] J.A. Langa, J.C. Robinson, and A. Suarez, Stability, instability and bifurcation phenomena in non-autonomous differential equations, *Nonlinearity* **15 (3)** (2002), pp. 887–903.
- [21] ———, Bifurcation in non-autonomous scalar equations, *J. Differential Equations* **221(1)** (2006), pp. 1–35.
- [22] T. Lenton, H. Held, E. Kriegler, J. Hall, W. Lucht, S. Rahmstorf, and H. Schellnhuber, Tipping elements in the Earth’s climate system, *Proceedings of the National Academy of Sciences of the United States of America* **105(6)** (2008), 1786–1793.
- [23] K. Palmer, The structurally stable systems on the half-line are those with exponential dichotomy, *J. Diff. Eqn.* **33** (1979), pp. 16–25.

- [24] C. Perryman and S. Wieczorek, Adapting to a changing environment: non-obvious thresholds in multi-scale systems, Proceedings of the Royal Society A: Mathematical, Physical and Engineering Science **470** (2014), no. 2170, 20140226.
- [25] C. Pötzsche, Nonautonomous bifurcation of bounded solutions i: A lyapunov-schmidt approach, Discrete and Continuous Dynamical Systems -Series B **14(2)** (2010), pp. 739–776.
- [26] ———, Bifurcations in nonautonomous dynamical systems: Results and tools in discrete time, Proceedings of the International Workshop Future Directions in Difference Equations (2011), pp. 163–212.
- [27] ———, Bifurcations in nonautonomous dynamical systems: Results and tools in discrete time, Proceedings of the International Workshop Future Directions in Difference Equations (2011), pp. 163–212.
- [28] ———, Persistence and imperfection of nonautonomous bifurcation patterns, Journal of Differential Equations **250(10)** (2011), pp. 3874–3906.
- [29] M. Rasmussen, Attractivity and bifurcation for nonautonomous dynamical systems, Lecture Notes in Mathematics, vol. 1907, Springer, 2007.
- [30] ———, Finite-time attractivity and bifurcation for nonautonomous differential equations, Differential Equations and Dynamical Systems **18** (2010), pp. 57–58.
- [31] M. Scheffer, Critical Transitions in Nature and Society, Princeton University Press, Princeton, USA, 2009.
- [32] Peter Szmolyan and Martin Wechselberger, Canards in \mathbb{R}^3 , Journal of Differential Equations **177** (2001), no. 2, 419 – 453.
- [33] Martin Wechselberger, Canards, Scholarpedia **2** (2007), no. 4, 1356.
- [34] Sebastian Wieczorek, Peter Ashwin, Catherine M Luke, and Peter M Cox, Excitability in ramped systems: the compost-bomb instability, Proceedings of the Royal Society of London A: Mathematical, Physical and Engineering Sciences **467** (2011), no. 2129, 1243–1269.

A Algorithm for approximation of spectral quantities

Consider the initial value problem

$$\begin{cases} \dot{x}(t) = f(x(t), \lambda(t)) \\ x(0) = x_0 \end{cases} \quad (14)$$

and the associated linear variational equation

$$\dot{u} = A(t)u \quad (15)$$

where $A(t) = Df(x(t), \lambda(t))$ and $D = \partial/\partial x$. For a given fundamental matrix solution $X(t)$ of (15) we define d upper characteristic exponents by the formulas

$$\mu_i(X) = \limsup_{t \rightarrow \infty} \frac{1}{t} \ln |X(t)e_i|, \quad i = 1, \dots, d \quad (16)$$

where e_i is the i th standard basis vector. The d lower characteristic exponents of X are defined by replacing the limsup with a liminf in (16). The upper (resp. lower) Lyapunov exponents of (15) are the upper (resp. lower) characteristic exponents whose sum is minimized (resp. maximized) over all fundamental matrix solutions. Letting $\lambda_1 \geq \lambda_2 \geq \dots \geq \lambda_d$ denote the ordered lower Lyapunov exponents and $\mu_1 \geq \mu_2 \geq \dots \geq \mu_d$ denote the order upper Lyapunov exponents, we define the Lyapunov spectrum Σ_L of (15) as

$$\Sigma_L := [\lambda_1, \mu_1] \cup [\lambda_2, \mu_2] \cup \dots \cup [\lambda_d, \mu_d].$$

Lyapunov's Theorem proves that the optimization problems define the Lyapunov spectrum always has a solution and that, if $\Sigma_L \cap [0, \infty) = \emptyset$, then the equilibrium at zero of (15) is asymptotically stable. Conversely, if $\Sigma_L \cap [0, \infty) \neq \emptyset$, then the equilibrium at zero is unstable. Under additional mild hypotheses, the Lyapunov stability (or instability) of the equilibrium of (15) implies the Lyapunov stability (or instability) of the solution $x(t; x_0)$ of the non linear problem

Determining exact expressions for the Lyapunov exponents of a given problem is not generally possible. Therefore we rely on robust numerical methods to approximate them. Given a fundamental matrix solution $X(t)$ of (15) we can form a unique smooth QR factorization $X(t) = Q(t)R(t)$ where $Q(t) \in \mathbb{R}^{d \times d}$ is orthogonal and $R(t) \in \mathbb{R}^{d \times d}$ is upper triangular with positive diagonal entries. $Q(t)$ satisfies the differential equation

$$\dot{Q}(t) = Q(t)S(Q(t), A(t)), \quad S(Q, A)_{ij} = \begin{cases} (Q^T A Q)_{ij}, & i > j \\ 0, & i = j \\ -(Q^T A Q)_{ji}, & i < j \end{cases}$$

and $R(t)$ satisfies the matrix differential equation $\dot{R} = B(t)R$ where $B(t) = Q^T(t)A(t)Q(t) - Q^T(t)\dot{Q}(t)$ is upper triangular for all t . Under the generic (see [23]) assumption that the system $\dot{y}(t) = B(t)y(t)$ has an integral separation structure, Theorem 5.1 of [10] implies that the Lyapunov spectrum of (15) is given by

$$\lambda_i = \liminf_{t \rightarrow \infty} \frac{1}{t} \int_0^t B_{i,i}(\tau) d\tau, \quad \mu_i = \limsup_{t \rightarrow \infty} \frac{1}{t} \int_0^t B_{i,i}(\tau) d\tau, \quad i = 1, \dots, d. \quad (17)$$

For $t > 0$ and $H \geq 0$ define the quantities

$$\mu_i^B(t, H) = \frac{1}{H} \int_t^{t+H} B_{i,i}(\tau) d\tau, \quad i = 1, \dots, d \quad (18)$$

where by convention we take $\mu_i^B(t, H) = B_{i,i}(t)$ if $H = 0$ for $i = 1, \dots, d$. The quantities (18) are referred to as Steklov averages in the literature and we refer to the quantity $\mu_i^B(t, H)$ as the i^{th} Steklov average of (15) of window length H at time t . The quantities $\mu_i^B(t, H)$ provides a measure for the exponential growth or decay rate of perturbed trajectories on the interval $[t, t+H]$ or more heuristically, they measure the attractivity and repulsivity of the solution $x(t; x_0)$. In other words $\mu_i^B(t, s)$ is an approximate local or finite-time Lyapunov exponent.

Consider the extended system

$$\begin{cases} \dot{x} = f(x, t) \\ \dot{Q} = QS(Q, A) \end{cases} \quad (19)$$

If we use the solution of (19) with $x(0) = x_0$ and some random orthogonal $Q_0 \in \mathbb{R}^{d \times d}$ to form $B(t) = Q(t)^T A(t)Q(t) - Q(t)^T \dot{Q}(t)$, then generically the Lyapunov exponents are given by equation (17). Additionally the first p columns of Q align to form a basis for the Lyapunov vectors corresponding to the largest p upper Lyapunov exponents. A unit vector v is a Lyapunov vector for the Lyapunov exponent μ if the solution of $\dot{x} = f(x, t)$ through an initial condition perturbed in the direction v separates from the unperturbed trajectory at a rate of $e^{\lambda t}$.

There are two alternative methods to computing the solution of (19) called respectively the continuous QR and discrete QR methods. We remark that the continuous and discrete QR methods are theoretically equivalent and the choice as to which method to use depends upon the problems. The discrete QR method may be preferable in situations where $A(t)$ becomes badly scaled or if the differential equation $\dot{Q} = QS(Q, A)$ becomes overly stiff.

The continuous QR method is to directly integrate the system (19) using some numerical method making sure to maintain the orthogonality of $Q(t)$ by either using an orthogonality preserving numerical scheme or projecting the approximated value Q_n of $Q(t_n)$ at each time step t_n to the nearest orthogonal matrix. Alternatively, the discrete QR method is as follows. Suppose that x_n and Q_n are the approximations of the solutions $x(t)$ and $Q(t)$ of (19) at the time t_n . We then continue the numerical solution of $\dot{x} = f(x, t)$ to find x_{n+1} and let $X_n \approx X(t_{n+1}, t_n)$ where $X(t, t_n)$ is the solution of the matrix differential equation initial value problem $\dot{\Psi}(t) = A(t)\Psi$, $\Psi(t_n) = I$. We then form the QR factorization of $X_n Q_n$ as $X_n Q_n = Q_{n+1} R_n$ where Q_{n+1} is orthogonal and R_n is upper triangular with positive diagonal entries.

Algorithm: Approximation of upper and lower Lyapunov exponents and Steklov averages

input : $x_0, Q_0, T_0 > 0, T_f > T_0, H > 0$

output: Approximate values: $\lambda_i(T_0, T_f) \approx \lambda_i, \mu_i(T_0, T_f) \approx \mu_i, s_i(t, H) \approx \mu_i^B(t, H)$, where $i = 1, \dots, d$

Solve (19) on the interval $[0, T_f]$ using either the continuous or discrete QR method with the initial condition $x(0) = x_0, Q(0) = Q_0$ to get $x(t), Q(t)$;

For $t \in [0, T_f]$ set $A(t) := Df(x(t; x_0), \lambda(t))$ and $\dot{Q}(t) := Q(t)S(Q(t), A(t))$, and

$B(t) = Q^T(t)A(t)Q(t) - Q(t)^T\dot{Q}(t)$;

for $i \leftarrow 1 : d$ **do**

 Set $s_i(t, H)$ to be an approximation to the integral $\frac{1}{H} \int_t^{t+H} B_{i,i}(\tau) d\tau$ for $t \in [0, T_f - H]$;

 Set $I_i^B(t)$ to be an approximation to the integral $\frac{1}{t} \int_0^t B_{i,i}(\tau) d\tau$ for $t \in [T_0, T_f]$;

 Set $\lambda_i(T_0, T_f) := \min_{t \in [T_0, T_f]} I_i^B(t)$ and $\mu_i(T_0, T_f) := \max_{t \in [T_0, T_f]} I_i^B(t)$

end

We use the following algorithm for the approximation of upper and lower Lyapunov exponents and Steklov averages. We can easily add the columns of $Q(t)$ to the output of the algorithm if we desire approximations to a basis for the Lyapunov vectors. We also remark that to solve the equation (19), we must have access to the function $Df(x, t)$ or at least an approximation to it since the differential equations that define $Q(t)$ depend on $A(t) = Df(x(t; x_0), t)$.

B Melnikov Integral Calculation

In this appendix we prove the following theorem.

Theorem 1. *The family of systems*

$$\begin{aligned}\dot{x}(t) &= -(x(t) - \lambda(t))(x(t) - \lambda(t) - \delta) \\ \dot{\lambda}(t) &= (a_* + \epsilon)\lambda(t)(1 - \lambda(t))\end{aligned}\tag{20}$$

with $\delta \in (0, 1)$ and

$$a_* = \frac{\delta^2}{(1 - \delta)}$$

has a unique heteroclinic orbit when $\epsilon = 0$.

The proof follows from several lemmas which are detailed below. The first lemma shows the existence of a heteroclinic connection when $\epsilon = 0$. The second lemma gives us the unique bounded solution to the adjoint variational equation, which we will need in the proof of the theorem. The proof of the theorem ultimately relies on a Melnikov integral calculation for the system which is needed to show that the heteroclinic orbit is unique. We follow the general outline that Homburg and Sandstede [?] use to show bifurcations in homoclinic orbits. The reader will note that their discussion is general enough to apply to heteroclinic orbits as well.

Lemma 2. *Assume that $\epsilon = 0, \delta \in (0, 1)$ and $a_* = \delta^2/(1 - \delta)$ in the system given by (20). Then the heteroclinic connection for the system is given by the line segment between $(\delta, 0)$ and $(1, 1)$.*

Proof. First we find the equilibria of the system and show that two of these equilibria are hyperbolic. Then we will show that the line segment connecting these hyperbolic equilibria coincides with the stable and unstable subspaces at the equilibria in that the segment is invariant. This shows that the line segment is in fact a heteroclinic connection between the equilibria.

The system has four equilibria, $(0, 0)$, $(\delta, 0)$, $(1, 1)$ and $(1 + \delta, 1)$ and the linearization of the system is $\dot{u} = A(x, \lambda, a_*, \delta)u$ where $u = (x, \lambda)^T$ and the Jacobians at these four equilibria are

$$A(0, 0, a_*, \delta) = \begin{bmatrix} \delta & -\delta \\ 0 & a_* \end{bmatrix}, \quad A(\delta, 0, a_*, \delta) = \begin{bmatrix} -\delta & \delta \\ 0 & a_* \end{bmatrix}, \quad A(1, 1, a_*, \delta) = \begin{bmatrix} \delta & -\delta \\ 0 & -a_* \end{bmatrix},$$

$$A(1 + \delta, 1, a_*, \delta) = \begin{bmatrix} -\delta & \delta \\ 0 & -a_* \end{bmatrix}$$

Then $(\delta, 0)$ and $(1, 1)$ are hyperbolic equilibria because a_* and δ have the same sign for $\delta \in (0, 1)$.

Note that $A(\delta, 0, a_*, \delta)$ has eigenvalues $\mu_1 = -\delta$ and $\mu_2 = a_*$ and corresponding eigenvectors

$$v_1 = \begin{bmatrix} 1 \\ 0 \end{bmatrix}, \quad v_2 = \begin{bmatrix} \delta \\ \delta + a_* \end{bmatrix},$$

and $A(1, 1, a_*, \delta)$ has eigenvalues $\tilde{\mu}_1 = \delta$ and $\tilde{\mu}_2 = -a_*$ and the same eigenvectors. Thus the eigenspaces are parallel and only intersect when they coincide. From these eigenvectors we see that the equation for the line parallel to the unstable eigenspace through $(\delta, 0)$ is

$$\lambda = \frac{a_* + \delta}{\delta}(x - \delta),$$

and the line through $(1, 1)$ is

$$\lambda = \frac{a_* + \delta}{\delta}(x - 1) + 1.$$

These lines will coincide when $(1, 1)$ lies on the first line or $(\delta, 0)$ lies on the second. This occurs when

$$1 = \frac{a_* + \delta}{\delta}(1 - \delta)$$

which corresponds to the condition that $a_* = \delta^2/(1 - \delta)$ as was assumed.

Now we will show that the line segment between $(\delta, 0)$ and $(1, 1)$ is invariant. A point on the line segment between $(\delta, 0)$ and $(1, 1)$ is given by

$$\lambda = \frac{a_* + \delta}{\delta}(x - \delta) = \frac{\frac{\delta^2}{1-\delta} + \delta}{\delta}(x - \delta) = \frac{1}{1 - \delta}(x - \delta) \quad (21)$$

Since $\lambda(t)$ solves a logistic differential equation, let

$$\lambda_*(t) = \frac{e^{a_* t}}{\lambda_1 + e^{a_* t}}. \quad (22)$$

where $\lambda_1 = (1 - \lambda_0)/\lambda_0$ and $\lambda_0 = 10^{-6}$. Substituting into (21), we get

$$x_*(t) = (1 - \delta)\lambda_*(t) + \delta = \frac{\delta\lambda_1 + e^{a_* t}}{\lambda_1 + e^{a_* t}}. \quad (23)$$

Notice that $x_*(t) \rightarrow \delta$ as $t \rightarrow -\infty$ and $x_*(t) \rightarrow 1$ as $t \rightarrow \infty$. Furthermore, we have that $\lambda_*(t) \rightarrow 0$ as $t \rightarrow -\infty$ and $\lambda_*(t) \rightarrow 1$ as $t \rightarrow \infty$. If we can ensure that $x_*(t)$ satisfies the \dot{x} equation, then we will have shown that this line segment is invariant for the system.

We see that a time derivative calculation of the representation for x in equation (23) yields

$$\begin{aligned} \dot{x}_*(t) &= \frac{(\lambda_1 + e^{a_* t})\alpha_* e^{a_* t} - (\delta\lambda_1 + e^{a_* t})a_* e^{a_* t}}{(\lambda_1 + e^{a_* t})^2} \\ &= \frac{\delta^2 \lambda_1 e^{a_* t}}{(\lambda_1 + e^{a_* t})^2}. \end{aligned}$$

Furthermore, plugging equation (22) and equation (23) into the righthand side of the first line of (20) yields

$$\begin{aligned} -(x_* - \lambda_*)(x_* - \lambda_* - \delta) &= -\left(\frac{\delta\lambda_1}{\lambda_1 + e^{a_* t}}\right)\left(\frac{\delta\lambda_1}{\lambda_1 + e^{a_* t}} - \delta\right) \\ &= -\left(\frac{\delta\lambda_1}{\lambda_1 + e^{a_* t}}\right)\left(\frac{-\delta e^{a_* t}}{\lambda_1 + e^{a_* t}}\right) \\ &= \frac{\delta^2 \lambda_1 e^{a_* t}}{(\lambda_1 + e^{a_* t})^2} \end{aligned}$$

so x_* is a solution to the \dot{x} equation and the line is invariant. \square

This shows the existence of a heteroclinic orbit. In order to show that it's unique we'll need another lemma.

Lemma 3. *Assume $\epsilon = 0$, then the unique bounded solution to the adjoint variational equation for system (20) is given by*

$$\begin{bmatrix} x(t) \\ \lambda(t) \end{bmatrix} = \begin{bmatrix} (\lambda_1 + 1)^{2\delta/a_*} \left[\frac{e^{a_* t}}{(\lambda_1 + e^{a_* t})^2} \right]^{\delta/a_*} \\ -(1 - \delta)(\lambda_1 + 1)^{2\delta/a_*} \left[\frac{e^{a_* t}}{(\lambda_1 + e^{a_* t})^2} \right]^{\delta/a_*} \end{bmatrix} \quad (24)$$

Proof. The variational equation centered on the heteroclinic orbit (x_*, λ_*) for system (20) with $\epsilon = 0$ is

$$\begin{aligned} \dot{x} &= [2(\lambda_* - x_*) + \delta](x - \lambda) \\ \dot{\lambda} &= a_*(1 - 2\lambda_*)\lambda \end{aligned}$$

so the adjoint equation is

$$\begin{aligned} \dot{x} &= -[2(\lambda_* - x_*) + \delta]x \\ \dot{\lambda} &= [2(\lambda_* - x_*) + \delta]x - a_*(1 - 2\lambda_*)\lambda \end{aligned}$$

Substituting (x_*, λ_*) into the \dot{x} equation yields

$$\dot{x} = -[2(\lambda_* - x_*) + \delta]x = \left[\frac{2\delta\lambda_1}{\lambda_1 + e^{a_* t}} - \delta \right] x = \left[\frac{\delta\lambda_1 - \delta e^{a_* t}}{\lambda_1 + e^{a_* t}} \right] x.$$

We can solve this last form of the \dot{x} equation by separation of variables, for which the general solution is

$$x(t) = C \left[\frac{e^{a_* t}}{(\lambda_1 + e^{a_* t})^2} \right]^{\delta/a_*}.$$

Without loss of generality, let $x(0) = 1$, then $C = (\lambda_1 + 1)^{2\delta/a_*}$. Notice that x is bounded for all time.

We are now able to solve for λ . The $\dot{\lambda}$ equation is

$$\dot{\lambda} = -\dot{x} - \alpha_*(1 - 2\lambda_*)\lambda$$

which is of the form

$$\dot{\lambda} + b(t)\lambda = r(t)$$

where $b(t) = a_*(1 - 2\lambda_*(t))$ and $r(t) = -\dot{x}(t)$. Then the solution is

$$y(t) = De^{-B(t)} + e^{-B(t)} \int r(t)e^{B(t)}$$

where $B'(t) = b(t)$.

We see that

$$B(t) = \ln \left(\frac{e^{a_* t}}{(\lambda_1 + e^{a_* t})^2} \right)$$

so that

$$e^{\pm B(t)} = \left(\frac{e^{a_* t}}{(\lambda_1 + e^{a_* t})^2} \right)^{\pm 1}$$

and

$$\begin{aligned} \int r(t)e^{B(t)} &= - \int \dot{x} \left(\frac{x}{C} \right)^{a_*/\delta} dt \\ &= - \frac{1}{C^{a_*/\delta} \left(\frac{a_*}{\delta} + 1 \right)} x^{\frac{a_*}{\delta} + 1} \\ &= -(1 - \delta)C \left[\frac{e^{a_* t}}{(\lambda_1 + e^{a_* t})^2} \right]^{1/\delta}. \end{aligned}$$

Then the general solution for λ is

$$\begin{aligned}\lambda(t) &= \frac{D(\lambda_1 + e^{a_*t})^2}{e^{a_*t}} - (1 - \delta)C \frac{(\lambda_1 + e^{a_*t})^2}{e^{a_*t}} \left[\frac{e^{a_*t}}{(\lambda_1 + e^{a_*t})^2} \right]^{1/\delta} \\ &= \frac{D(\lambda_1 + e^{a_*t})^2}{e^{a_*t}} - (1 - \delta)x(t)\end{aligned}$$

Recall that we need λ to be bounded. If $D \neq 0$ then the solution $\lambda(t)$ will blow up, so D must be 0. Then

$$\lambda(t) = -(1 - \delta)x(t)$$

which gives us equation (24). Since $x(t)$ is bounded for all time, $\lambda(t)$ is also bounded. \square

We are finally ready to prove the theorem. Note that the proof relies on a Melnikov integral calculation. Recall that Melnikov integrals give the distance between stable and unstable manifolds associated with heteroclinic or homoclinic orbits. In the proof we will be calculating the distance between the stable manifold for $(1, 1)$ and the unstable manifold for $(\delta, 0)$. We will ultimately show that for the Melnikov integral is nonzero for $\epsilon \neq 0$. This means that if $\epsilon \neq 0$ then the distance between the stable and unstable manifolds is nonzero and there is no longer a heteroclinic connection.

Proof. (Theorem 1)

Let W_ϵ^u be the unstable manifold coming from the equilibrium at $(\delta, 0)$ and W_ϵ^s be the stable manifold coming from the equilibrium at $(1, 1)$ for some ϵ small. We define

$$\begin{aligned}W_\epsilon^u \cap \{\lambda = 0.5\} &= h^u(0; \epsilon) \\ W_\epsilon^s \cap \{\lambda = 0.5\} &= h^s(0; \epsilon).\end{aligned}$$

Any heteroclinic orbits near the heteroclinic orbit at a_* will have $h^u(0; \epsilon) = h^s(0; \epsilon)$. At $\epsilon = 0$, $t = 0$ we define the tangent spaces of the manifolds:

$$\begin{aligned}E_+ &= T_{x_*} W_0^u(\delta, 0) \\ E_- &= T_{x_*} W_0^s(1, 1).\end{aligned}$$

Notice that in our case $E_+ = E_-$ are the eigenspaces. Let $E_0 = E_+ \cap E_-$, we see that $E_0 = \text{span}\{(\delta, \delta + a_*)^T\}$. Also let $Z = (E_+ + E_-)^\perp$ to be an arbitrary complement. For now we will not specify Z .

For each ϵ close to zero, the orbits $h^u(\cdot; \epsilon)$ and $h^s(\cdot; \epsilon)$ satisfy $W_\epsilon^{s/u} = \text{graph}(h^{s/u})$,

$$h^{s/u} : E_0 \rightarrow Z$$

and $h^u(\cdot; 0) = h^s(\cdot; 0)$ is the heteroclinic orbit given in Lemma 2. We can use a Melnikov Integral to find the distance between h^s and h^u . In particular, at $t = 0$ we have

$$h^u(0, \epsilon) - h^s(0, \epsilon) = \int_{-\infty}^{\infty} \langle \psi(t), f_\epsilon(x_*, \lambda_*) \rangle dt$$

where ψ is the unique bounded solution to the adjoint variational equation with $\psi(0) \in Z$ and f_ϵ is the derivative with respect to ϵ of the righthand side of system (20). We see

$$f_\epsilon(x_*, \lambda_*) = \begin{bmatrix} 0 \\ \lambda_*(t)(1 - \lambda_*(t)) \end{bmatrix}$$

Also, recall that we found ψ in Lemma 3, but here we must ensure that the initial conditions are not in E_0 . Notice that $\psi(0) = (1, \delta - 1)^T$ which is transverse to $(\delta, \delta + a_*)$ (in fact it is perpendicular), so we take $Z = \text{span}\{(1, \delta - 1)^T\}$.

We now return to the Melnikov integral

$$\begin{aligned}\int_{-\infty}^{\infty} \langle \psi(t), f_{\epsilon}(x_*, \lambda_*) \rangle dt &= -(1 - \delta)C \int_{-\infty}^{\infty} \left[\frac{e^{a_* t}}{(\lambda_1 + e^{a_* t})^2} \right]^{\delta/a_*} \left[\frac{\lambda_1 e^{a_* t}}{(\lambda_1 + e^{a_* t})^2} \right] dt \\ &= -(1 - \delta)C \int_{-\infty}^{\infty} \left[\frac{e^{\delta t}}{(\lambda_1 + e^{a_* t})^{2\delta/a_*}} \right] \left[\frac{\lambda_1 e^{a_* t}}{(\lambda_1 + e^{a_* t})^2} \right] dt\end{aligned}$$

Notice that the integrand is strictly positive, so the resulting integral is strictly negative. This tells us that the heteroclinic connection found in Lemma 2 is unique. \square